RSC Advances

PAPER

View Article Online
View Journal | View Issue

Cite this: *RSC Adv.*, 2022, **12**, 4417

Chitin/egg shell membrane@Fe_3O_4 nanocomposite hydrogel for efficient removal of Pb^{2+} from aqueous solution†

Baoquan Jia,*[ac] Dingna Liu,[b] Chengyu Niu,[b] Qili Yu,[c] Jie Ren,[d] Qingye Liu *[b] and Haiqiang Wang [a]

The development of adsorbents by using the byproducts or waste from large-scale industrial and agricultural production is of great significance, and is considered to be an economic and efficient strategy to remove the heavy metals from polluted water. In this work, a novel chitin/EM@Fe_3O_4 nanocomposite hydrogel was obtained from a NaOH/urea aqueous system, where the proteins of egg shell membrane and Fe_3O_4 nanoparticles were chemically bonded to chitin polymer chains with the help of epichlorohydrin. Due to the existence of a large number of $-NH_2$, –OH, –CONH–, –COOH and hemiacetal groups, the adsorption efficiency for Pb^{2+} into the absorbent was dramatically enhanced. The experimental results revealed that the adsorption behavior strongly depends on various factors, such as initial pH, initial Pb^{2+} concentration, incubation temperature and contact time. The kinetic experiments indicated that the adsorption process for Pb^{2+} in water solution agreed with the pseudo-second-order kinetic equation. The film diffusion or chemical reaction is the rate limiting process in the initial adsorption stage, and the adsorption of Pb^{2+} into the nanocomposite hydrogel can well fit the Langmuir isotherm. Thermodynamic analysis demonstrated that such adsorption behaviors were dominated by an endothermic ($\Delta H^\circ > 0$) and spontaneous ($\Delta G^\circ < 0$) process.

Received 30th November 2021
Accepted 28th January 2022

DOI: 10.1039/d1ra08744d

rsc.li/rsc-advances

1. Introduction

In response to the national policy on the energy saving and carbon emission reduction, the electric car/bicycle industries have developed rapidly in recent years especially in China. As one of the most important parts, the battery has been paid great attention. Among those various batteries, the lead acid battery is still considered to be an essential species and widely used, due to its high stability, reliability and low cost. However, the extensive use and potential leakage of Pb^{2+} ions in the related industries, such as smelting, battery recycling, painting and mining, can result in high levels of contamination in water and thus accumulation *via* the food chain. Even very low levels of Pb^{2+} intake can give rise to serious irreversible injuries on human beings' nervous system, reproductive system, immune system, and organs.[1,2] Hence, effective removal of Pb^{2+} from industrial wastewater will contribute to environmental sustainability.

Up to now, diverse remediation technologies have been introduced to remove Pb^{2+} from wastewater, such as chemical reduction, electrocoagulation, ion exchange, membrane separation as well as adsorption.[3–6] Of the current strategies, adsorption has emerged as an effective way for water treatment due to its many advantages, including cost-efficiency, easy handling, availability of plentiful adsorbents and environment-friendly manner. Numerous absorbents, such as activated carbon, polymeric and lignocellulosic materials, inorganic nanoparticles and organic frameworks have been well developed to absorb the heavy metal ions from the aquatic environments.[7–13] Recently, concerns have been devoted into the utilization of biomass and agricultural wastes to remove heavy metal ions, where these adsorbents are usually derived from the byproducts or wastes from large-scale industrial and agricultural production.[13–15] Such behavior is of high significance for the developing countries, since huge amounts of agricultural wastes have been effectively recycled for the sake of saving the natural resources. For example, the orange and cucumber peels have been employed to treat the contaminated water.[14,16] The presence of carboxyl, hydroxyl, and carbonyl groups is likely responsible for the efficient adsorption of heavy metal ions. Egg shell membrane (EM) is a naturally-occurring biomaterial

[a]*Key Laboratory of Environment Remediation and Ecological Health, Ministry of Education, College of Environmental & Resources Science, Zhejiang University, Hangzhou, 310058, China. E-mail: baoquanjia@foxmail.com*

[b]*School of Chemical Engineering and Technology, North University of China, No. 3 Xueyuan Road, Jiancaoping District, Taiyuan, 030051, China. E-mail: qingyeliu@126.com*

[c]*Hangzhou Xiaoshan Donghai Breeding Co., Ltd, Hangzhou, 311200, China*

[d]*School of Environment and Safety Engineering, North University of China, No. 3 Xueyuan Road, Jiancaoping District, Taiyuan, 030051, China*

† Electronic supplementary information (ESI) available. See DOI: 10.1039/d1ra08744d

generated by poultry and regarded as a biowaste. This semi-permeable membrane is composed of the highly cross-linked protein fibers, and identified as a highly-value material in biomedical engineering benefitting from its nontoxic, collagen-rich and biocompatible characteristics.[16] Moreover, the unique 3D fibrous net-work and a large number of functional groups (–COOH, $–NH_2$ and –OH) would render the material with a strong ability to bind and capture metal ions.[17,18]

Chitin is another abundant and renewable biomass resource. It is composed of β-(1-4)-linked 2-acetamido-2-deoxy-D-glucose, and widely exists in different crustaceans, mollusks, algae, insects, fungi, and yeasts on earth.[19,20] The annual production of chitin is estimated to be about 10^{10} to 10^{11} tons from living organisms, and more than 10 000 tons could be available every year from shellfish wastes.[21] This polysaccharide possesses a number of amide (–NH–) and hydroxyl (–OH) groups in the polymer chains, which will facilitate the chelation to Ar^{3+}, Cd^{2+}, Co^{2+}, Cu^{2+}, Mn^{2+} and Pb^{2+} ions in aqueous system.[22] Thus, the chitin-derived materials as the low-cost absorbents have been largely applicated in the water treatment. This occurrence is further enhanced with the development of solvent systems of the chitin. The as-fabricated materials in terms of chitin fibers, crystals whisker, films, hydrogels, aerogels, microspheres and hybrid nanocomposites displayed high performance for the removal of heavy metal ions, organic dyes or pesticide.[21,23–25]

With respect to the advantages of these biomass resources, in this work, we aim to combine the chitin and egg shell membrane to create a novel kind of nanocomposite hydrogel to efficiently remove Pb^{2+} in an economical way. In the design, the magnetic Fe_3O_4 nanoparticles were also incorporated into the hydrogel matrix. On one hand, the Fe_3O_4 nanoparticles have a suitable framework for interaction with Pb^{2+}, leading to enhanced adsorption efficiency;[26] on the other hand, the introduction of magnetic particles could provide the convenience for the ultimate separation. Thus, the impacts of the environmental pH condition, initial Pb^{2+} concentration and incubation temperature on Pb^{2+} adsorption into the chitin/EM@Fe_3O_4 nanocomposite hydrogel were investigated in detail, respectively. The corresponding adsorption kinetics and isotherm behaviors were also explored. We believe that this work provides a promising strategy for the construction of novel biomass-based absorbents for rapid and high-capacity removal of heavy metal ions.

2. Experimental

2.1 Materials

Chitin powder with a degree of acetylation about 98% was purchased from Jinke Chitin Co. Ltd (Zhejiang, China). The weight-average molecular weight (M_w) of chitin was evaluated to be 5.0×10^5 by dynamic light scattering (DLS, ALV/CGS-8F, ALV, Germany) in 5% LiCl/DMAc (w/w). Raw egg shell membranes were collected from local school restaurants. All of the chemical reagents including NaOH, urea, HCl, $Pb(NO_3)_2$, epichlorohydrin, EDTA·2Na, H_2O_2 and alcohol were analytical grade from commercial sources in China. Trisodium citrate dihydrate, $FeCl_3 \cdot 6H_2O$, NaAc, ethylene glycol were obtained from Aladdin Chemical Co. Ltd (Shanghai, China).

2.2 Preparation of highly water-dispersible Fe_3O_4 nanoparticles

The magnetite Fe_3O_4 nanoparticles were prepared through a modified solvothermal reaction.[27] Briefly, 2.025 g of $FeCl_3 \cdot 6H_2O$, 5.781 g of NaAc, and 0.684 g of trisodium citrate dihydrate were dissolved in 150 mL of ethylene glycol. After vigorous stir for 1 h at room temperature, the as-formed homogeneous black mixture was transferred into a Teflon-lined stainless-steel autoclave (200 mL) with the further incubation at 200 °C for 10 h. During the process Fe^{3+} was partly reduced into Fe^{2+}. Finally, the obtained Fe_3O_4 product was washed with ethanol for 6–10 times with the help of a magnet field, and then dried in oven at 60 °C for further use.

2.3 Pre-treatment of raw egg shell membranes

Raw egg shell membranes were obtained by peering manually from discarded eggshells and composed of both inner and outer membranes. Subsequently, the membranes were treated with HCl (5.0 wt%) for 4 h to remove the $CaCO_3$ residues, and thoroughly washed in deionized water. After incubation in 0.1 mmol L^{-1} EDTA aqueous solution for 24 h and fully rinse with deionized water, the fresh egg shell membranes (denoted as EM) were collected. These products were finally dried at 60 °C and ground into powders for the preparation of nanocomposite hydrogels.

2.4 Fabrication of the chitin/EM@Fe_3O_4 nanocomposite hydrogel

The fabrication of chitin/EM@Fe_3O_4 nanocomposite hydrogel was mainly involved two steps, the dissolution of egg shell membranes and chitin in NaOH/urea solvent system. Firstly, 1.0 g EM powders were totally dissolved into 11.0 wt% NaOH aqueous solution upon heating and sonification. After cooling down to room temperature, certain amount of urea was added to form the 1.0 wt% EM/11.0 wt% NaOH/4.0 wt% urea/80.0 wt% H_2O mixture system. Subsequently, 4.0 g chitin powders were dispersed into the above mixture solution with stirring for 5 min, and then was stored under refrigeration (−30 °C) for 4 h.[28] The frozen solid was thawed and stirred extensively at room temperature. After the freeze/thawing manipulation were repeated 3 cycles, 2.0 mL epichlorohydrin as cross-linker and 1.0 mL Fe_3O_4 aqueous dispersion were added into 100 g of the mixture solution and stirred at 0 °C for 0.5 h to obtain a homogeneous solution, which was then subjected to centrifugation for 10 min at 4 °C. In the following, the obtained uniform solution was cast into a Petri dish and kept at ambient temperature for 12 h allowing the gelation. Finally, the as-prepared hydrogel was immersed in distilled water for 3 days to remove any residues. The nanocomposite hydrogel sample was labeled as chitin/EM@Fe_3O_4. For the preparation of chitin and chitin/EM hydrogels, similar experimental procedures with a fixed concentration of epichlorohydrin (2.0 mL/100 g) were displayed. For the preparation of nanocomposite hydrogel

beads, the obtained pre-gel solution was allowed to drip into hot water by an injector to get the raw beads. After thorough washing with ultrapure water, the hydrogel beads were collected.

2.5 Adsorption behaviors studies

The adsorption behaviors of Pb^{2+} into chitin/EM@Fe_3O_4 hydrogel including the effects of environmental pH condition and incubation temperature, kinetic mechanisms, adsorption isotherms and thermodynamic parameters were explored intensively. All the experiments were performed in 50 mL plastic centrifuge tubes containing 30 mL of Pb^{2+} stock solution by utilizing the batch equilibrium method. During the whole process, all the tubes were sealed with the caps and placed in a thermostatic water bath shaker at a speed of 150 rpm. In the adsorption isotherm, the initial concentrations of Pb^{2+} varied from 0.5 to 20.0 mmol L^{-1} at the incubation temperature of 293 K. To each container, approximate 1.0 g hydrogel samples were added. After incubation for 24 h, the equilibrium concentration of Pb^{2+} in each tube was determined with ICP-OES spectrometer. Thus, the adsorption capacity, q_e (mmol g^{-1}), of Pb^{2+} into chitin/EM@Fe_3O_4 hydrogel can be calculated as:[29]

$$q_e = \frac{(c_0 - c_e)V}{W} \quad (1)$$

where c_0 and c_e are the initial and equilibrium concentrations of Pb^{2+} (mmol L^{-1}), respectively, V is the volume of Pb^{2+} aqueous solution (L) in each tube and W is the mass of chitin/EM@Fe_3O_4 hydrogel samples (g).

For the kinetic studies, 1.0 g chitin/EM@Fe_3O_4 hydrogel samples were added to 30 mL of Pb^{2+} aqueous solution. The concentration was kept at 5.0 mmol L^{-1} and the pH value was set to be 5.0. At different time intervals, the final concentration of Pb^{2+} in each container was analyzed by ICP-OES. To investigate the effect of pH on the Pb^{2+} adsorption capacity, the pH values were changed from 1.0 to 5.0 by adding diluted HCl solution. At higher pH condition, the Pb^{2+} ions are easy to precipitate. In order to investigate the impact of incubation temperature on the adsorption efficiency, the batch adsorption studies were performed at the temperatures of 277, 293 and 310 K, respectively.

2.6 Desorption and regeneration studies

In order to evaluate the desorption and regeneration abilities of chitin/EM@Fe_3O_4 hydrogel, 1.0 g samples were fistly placed in 30 mL of 5.0 mmol L^{-1} Pb^{2+} aqueous solution. After incubation for 24 h at 293 K, the adsorbents and aqueous solution were collected, respectively. The aqueous solution was used to evaluate the adsorption capacity and desorption efficiency. The adsorbents were regenerated by using 10 mL of 0.05 mol L^{-1} HCl as the static eluting solution for 3 times. Each static elution time was set to be 4 h. Then, the adsorbent was fully washed with deionized water for the subsequent adsorption studies. For comparison, the hydrogel samples were also regenerated by using 10 mL of 0.1 mol L^{-1} EDTA as the static eluting solution for 3 times. Each static elution time was set to be 4 h. After that, the adsorbent was fully washed by 1.0 mol L^{-1} NaCl solution and deionized water for the succeeding adsorption performance. This adsorption–desorption cycle in both cases was repeated 3 times under the same condition.

2.7 Characterization

The wide-angle X-ray diffraction (XRD) patterns for each sample were recorded in reflection mode on a Rigaku SmartLab diffractometer equipped with a CuKα radiation source (λ = 1.542 Å) operated at 40 kV and 30 mA. The samples were scanned at 4° min^{-1} and at a step size of 2.5° in 2θ. The FT-IR spectra were recorded in the wavenumber range from 4000 to 700 cm^{-1} using the attenuated total reflection Fourier transform infrared spectroscopy (ATR-FTIR, PerkinElmer, USA) at room temperature. The samples were freeze-dried in a conventional freezer dryer and then dried at 45 °C in a vacuum chamber to eliminate water from the samples. Thermogravimetric analysis (TGA) tests were performed on a TG instrument (PerkinElmer Co., USA) in an atmosphere of nitrogen at a heating rate of 10 °C min^{-1} from 50 to 650 °C. High resolution transmission electron microscopy (HR-TEM) and SAED images were acquired using a JEM-2011 transmission electron microscope (JEOL Ltd, Japan) operated at 200 kV. Magnetic characterization was carried out on a vibrating sample magnetometer (PPMS-9, Quantum Design, USA). Particle size and zeta potential were measured using a Nano-ZS ZEN3600 (Malvern Instruments, UK) at 25 °C. The exact concentration of Pb^{2+} in solution was determined by the ICP-OES instrument with an RF generator power 1150 W (Thermo, USA). The auxiliary, carrier and plasma gas (Ar) flow rates were set to be 0.5, 0.5 and 12.0 L min^{-1}, respectively. The wavelength of emission line for Pb is 220.353 nm. The leaching concentration of Fe^{2+}/Fe^{3+} in solution was determined by the ICP-MS instrument (Agilent 7700, USA), and the total weight content of Fe in chitin/EM@Fe_3O_4 hydrogel sample was measured by the ICP-OES instrument (Agilent 725ES, USA). The wavelength of emission line for Fe is 239.56 nm.

3. Results and discussion

3.1 Structure characterization of chitin/EM@Fe_3O_4 hydrogel

The prerequisite for preparation of chitin/EM@Fe_3O_4 nanocomposite hydrogel is the dissolution of both chitin and egg shell membrane in an appropriate solvent system. In the design, we attempted to fabricate this novel adsorbing material by dissolving them in the 11.0 wt% NaOH/4.0 wt% urea solvent system. One possible reason for the choice can be attributed to the fact that as-prepared hydrogel from the alkali/urea solvent system is expected to display excellent mechanical properties,[20] which will guarantee the stability and integrity of the absorbents in the recycle processing. During the whole preparation, egg shell membranes were firstly allowed to be dissolved in 11.0 wt% NaOH aqueous solution upon heating, and then the chitin powders were dispersed and finally dissolved in the 11.0 wt% NaOH/4.0 wt% urea solution *via* freeze–thawing cycle treatment. By addition of water-dispersible Fe_3O_4 nanoparticles

and chemical-crosslink agent of epichlorohydrin into the mixture, the chitin/EM@Fe_3O_4 nanocomposite hydrogel was obtained after thorough washing in water. As shown in Fig. 1a, the hydrogel samples showed different morphologies. The pure chitin hydrogel is transparent and colorless, while the chitin/EM hydrogel displays the yellowish color and higher swelling behavior, indicating the successful chemical crosslinking between EM protein and chitin polymer chains. By comparison, the chitin/EM@Fe_3O_4 nanocomposite hydrogel shows the dark-brown color, as a result of the existence of Fe_3O_4 nanoparticles in the matrix. Meanwhile, by immersing the nanocomposite hydrogel into water for 1 week, the Fe_3O_4 nanoparticles were hardly observed and separated from the hydrogel matrix, illustrating the strong affinity to the matrix and high stability of the bio-absorbents. It should be mentioned that we didn't adopt the fabrication strategy by *in situ* synthesis of Fe_3O_4 in the hydrogel matrix, because Fe^{3+} ions are not easy to penetrate into the deep interior of the hydrogel, finally leading to the gradient distribution of Fe_3O_4 in the matrix. This heterogeneous structure will display an adverse effect on the adsorption capacity.

The existence of Fe_3O_4 nanoparticles in the nanocomposite hydrogel was firstly studied using a vibrating sample magnetometer (shown in Fig. 1b). The results demonstrate that the nanocomposite hydrogel possesses a superparamagnetic character. Both the chitin/EM@Fe_3O_4 hydrogel samples and Fe_3O_4 nanoparticles had no remanence or coercivity at 300 K, and the magnetization saturation values (Ms) were evaluated to be 2.8 and 58.2 emu g^{-1}, respectively. The smaller Ms value can be ascribed to the lower content of Fe_3O_4 nanoclusters in the nanocomposite hydrogel. Nevertheless, the as-prepared hydrogel beads (shown in Fig. S1†) can be still easily separated from aqueous solution under an external magnetic field.

Further evidence was collected from the EDS pattern (Fig. 1c). The observation for the elements of Fe and O in the spectrum confirmed the successful synthesis of the magnetite particles. The particle size analysis and TEM images (Fig. 1d and e) reveal that the Fe_3O_4 particles have a uniform size of about 290 nm, and dispersed in the hydrogel matrix. The particles are composed of nanocrystals with the size of about 5–20 nm, where the nanocrystals seem to be connected with each other similar like the appearance of pomegranate. Selected-area

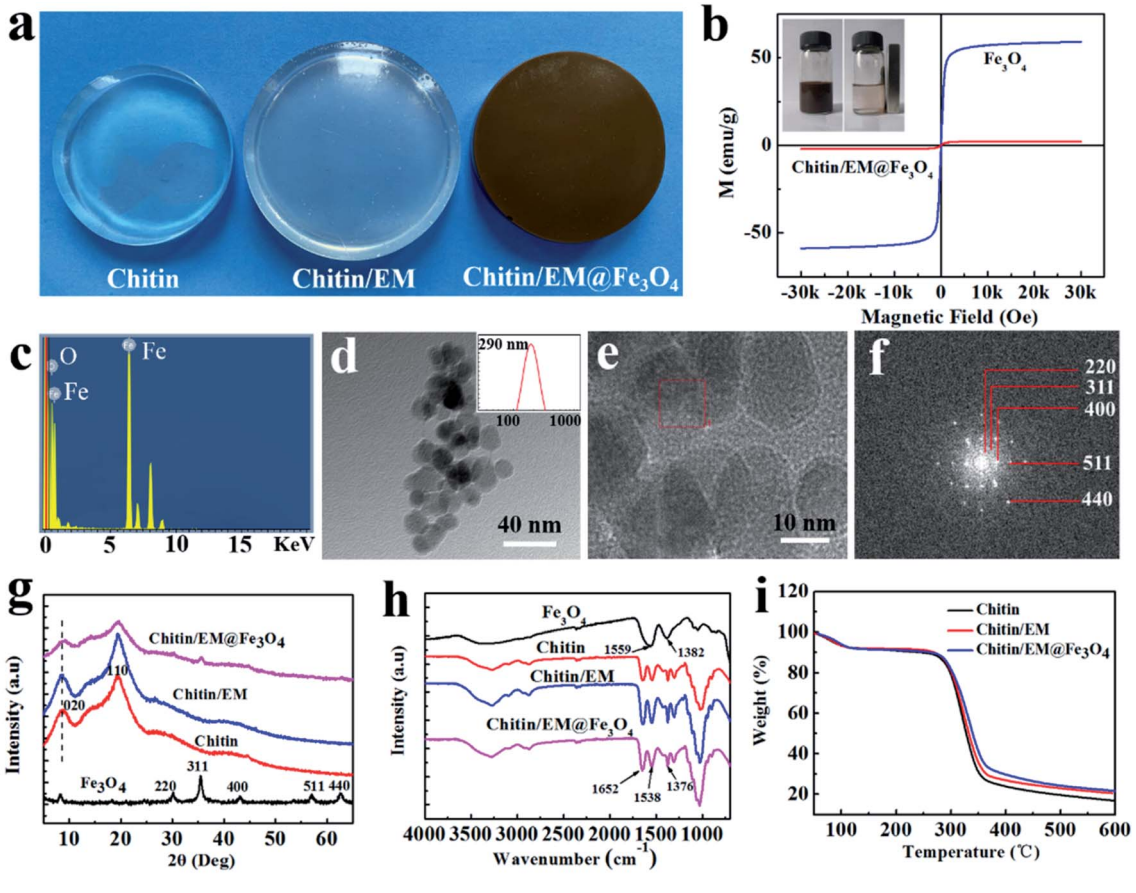

Fig. 1 (a) Photographs of the as-prepared hydrogel samples. (b) Magnetic hysteresis loops of Fe_3O_4 particles and chitin/EM@Fe_3O_4 hydrogel sample. (Inset) Pictures of Fe_3O_4 nanoparticles in aqueous solution before and after suffering from a magnetic field. (c) EDS spectra for the chitin/EM@Fe_3O_4 hydrogel sample. (d) TEM image and (e) high resolution TEM image of the Fe_3O_4 nanoparticles dispersed in chitin/EM@Fe_3O_4 hydrogel. (Inset) The corresponding size distribution of the Fe_3O_4 particles. (f) SAED pattern for the corresponding location. XRD patterns (g), TGA curves (h) and (i) FT-IR spectra for the specimens.

electron diffraction (SAED) (Fig. 1f) recorded on the edge of a magnetite particle presents the polycrystalline-like phase pattern. This structure may provide them with a large surface area for adsorption of guest molecules, such as the heavy metal ions or organic dyes.[30]

Fig. 1g presents the XRD patterns for Fe_3O_4, chitin, chitin/EM and chitin/EM@Fe_3O_4, respectively. The typical pattern of Fe_3O_4 particles exhibits the strong diffraction peaks at 2θ =30.1°, 35.4°, 43.1°, 57.0° and 62.7°, corresponding to the reflection planes of (220), (311), (400), (511) and (440), respectively. This result indicates that the magnetite particles possess the polycrystalline structure, which is in good agreement with the SAED. In the case of chitin pure hydrogel, two main semi-crystalline peaks at 2θ =8.6° and 19.4° occurred, which are assigned to the (020) and (110) reflections, respectively. For the chitin/EM nanocomposite hydrogel, it shows the similar diffraction behavior to the chitin, implying that the EM was greatly degraded into small peptide sections during the fabrication process. The occurrence of the diffraction peaks at 2θ =30.1° and 35.4° in the chitin/EM@Fe_3O_4 nanocomposite hydrogel samples proves that Fe_3O_4 particles have been well incorporated into the hydrogel matrix. In addition, the diffraction peak at 2θ =8.6° in the chitin/EM sample shifted to 9.3°. The strong interaction between the Fe_3O_4 particles and hydrogel polymer network and certain chemical-crosslink reaction may commonly contribute to this phenomenon. More information on the mutual interactions was identified from ATR-FTIR spectra (Fig. 1h). As shown, all the tested samples show the prominent absorption bands around 3287–3432 cm^{-1}, which are ascribed to the stretching mode of O–H and N–H groups. These features ensure that the EM proteins and Fe_3O_4 particles could be chemically bonded to chitin in presence of epichlorohydrin. The respective peaks in the nanocomposite hydrogel located at 1652 cm^{-1}, 1538 cm^{-1} and 1376 cm^{-1} mainly originate from the amide I, amide II and amide-III bands of chitin. The characteristic peaks at 1559 and 1382 cm^{-1} associated with carboxylate groups in the Fe_3O_4 particles shifted to the lower wavenumber region, and seem to be overlapped by the amide (II and III) bands, suggesting the strong hydrogen bonding interactions between Fe_3O_4 particles and the polymer chains. Thermogravimetric analysis (Fig. 1i) illustrate that the thermal stability of chitin/EM@Fe_3O_4 nanocomposite hydrogel was slightly enhanced by incorporation of EM and Fe_3O_4 particles. According to the percentage of weight loss in N_2 atmosphere, the contents for EM and Fe_3O_4 particles in the given nanocomposite system were estimated to be 23.1 wt% and 3.1 wt%, respectively.

3.2 Adsorption kinetics of Pb^{2+} into chitin/EM@Fe_3O_4 hydrogel

Fig. 2 presents the equilibrium adsorption capacity for Pb^{2+} into different adsorbents. As indicated, three hydrogel species displayed the differentiated efficiency. A relatively higher q_e value was observed in the chitin/EM hydrogel samples than chitin pure hydrogel, implying that the abundant groups such as the $-NH_2$ and –COOH in the EM protein will provide more

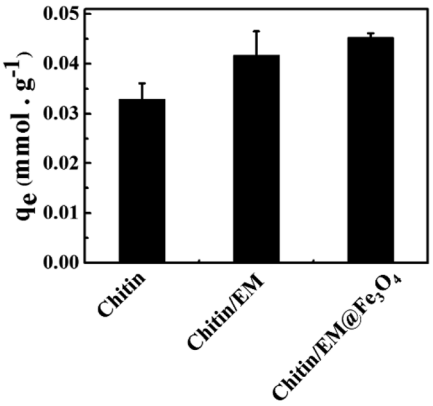

Fig. 2 The equilibrium adsorption capacity of Pb^{2+} in chitin, chitin/EM and chitin/EM@Fe_3O_4 hydrogels at 20 °C in pH = 5 aqueous solution.

feasibility to anchor the heavy metal ions. Among these adsorbents, the chitin/EM@Fe_3O_4 nanocomposite hydrogel showed the highest q_e value. The addition of Fe_3O_4 nanoparticles in the hydrogel matrix is favorable for the chelation to Pb^{2+} ions. The citrate stabilized Fe_3O_4 nanoparticles own a large number of –COOH groups on the surface.[30] Besides, the magnetite nanoparticles show the characteristics of high surface area and unique cubic inverse spinel structure. There features are conductive to the interactions with Pb^{2+} ions.[26] With respect to the improvement in adsorption capacity, the chitin/EM@Fe_3O_4 nanocomposite hydrogel can be taken as the promise candidate for water treatment.

The adsorption behaviors of Pb^{2+} into chitin/EM@Fe_3O_4 hydrogel were extensively investigated. Fig. 3a depicts the dependence of the q_e value for Pb^{2+} adsorption into nanocomposite adsorbent *versus* the incubation time in aqueous solution. The q_e increased almost linearly in the initial period, implying a quick and efficient adsorption process on the surface of chitin/EM@Fe_3O_4 hydrogel. Upon 24 h incubation, the biosorption equilibrium was established. The time profile for the Pb^{2+} uptake in water was smooth and continuous until the equilibrium, suggesting that the monolayer adsorption possibly occurred.[31] To analyze the adsorption kinetics of Pb^{2+} into the as-prepared nanocomposite hydrogel, several basic models including the pseudo-first-order, kinetics pseudo-second-order kinetics, and intraparticle diffusion models were applied. The related parameters obtained from these equations will cast great significance on how to design and model the adsorption process. The pseudo-first-order kinetic equation can be expressed as follows:[32]

$$\frac{1}{q_t} = \left(\frac{k_1}{q_1}\right)\left(\frac{1}{t}\right) + \frac{1}{q_1} \quad (2)$$

The pseudo-second-order kinetic model can be depicted as:[29]

$$\frac{t}{q_t} = \frac{1}{k_2 q_2^2} + \left(\frac{1}{q_2}\right)t \quad (3)$$

where q_t is the adsorption amount of Pb^{2+} (mmol g^{-1}) in chitin/EM@Fe_3O_4 hydrogel at different time t. q_1 (mmol g^{-1}) and k_1

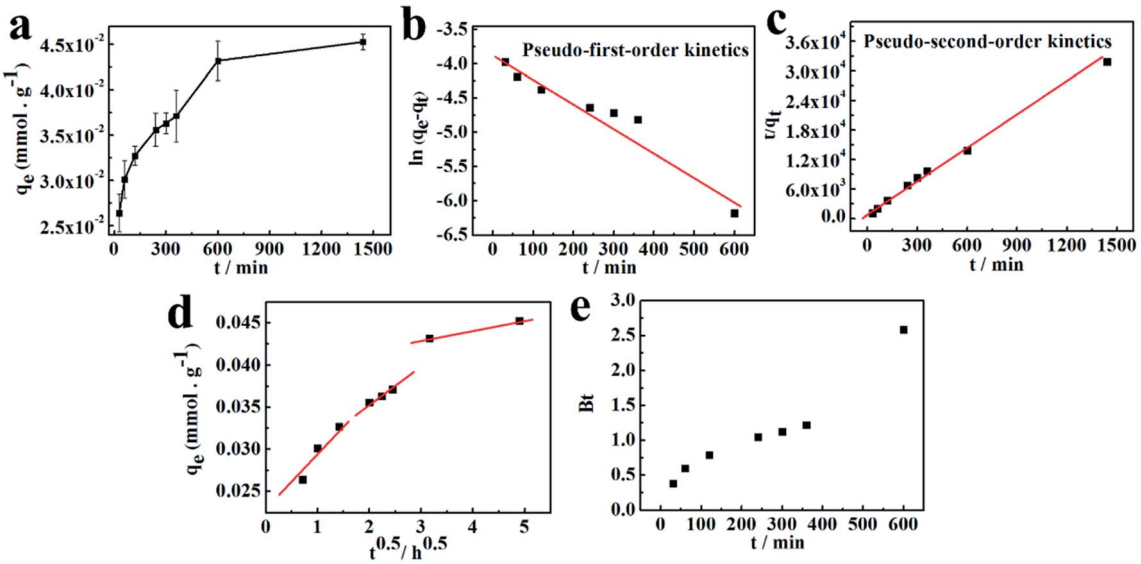

Fig. 3 (a) The effect of contact time on the Pb^{2+} adsorption in chitin/EM@Fe_3O_4 hydrogel at 20 °C in pH = 5 aqueous solution. The corresponding pseudo-first-order model (b), pseudo-second-order model (c), intra-particle diffusion plots (d) and (e) Boyd plots for Pb^{2+} adsorption in chitin/EM@Fe_3O_4 hydrogel at 20 °C in pH = 5 aqueous solution.

(h^{-1}) are the maximum adsorption capacity and rate constants for the pseudo-first-order model, while q_2 (mmol g^{-1}) and k_2 (g $mmol^{-1}$ h^{-1}) represent the maximum adsorption capacity and rate constants for the pseudo-second-order model. The values of k_1, k_2, q_1, q_2 and correlation coefficients of R_1^2 and R_2^2 for Pb^{2+} adsorption can be easily drawn from the linear fitting plots of $\ln(q_e - q_t)$ *versus* t (Fig. 3b) and t/q_t *versus* t (Fig. 3c), respectively. As listed in Table 1, the maximum adsorption capacity of q_2 for Pb^{2+} in aqueous solution is almost same to the actual experimental data (Fig. 3a). Meanwhile, the correlation coefficients (R_2^2) for pseudo-second-order kinetic model is 0.9966, which is much closer to 1.0. Hence, the adsorption in water solution follows the pseudo-second-order kinetic model, implying that Pb^{2+} adsorption in chitin/EM@Fe_3O_4 hydrogel is controlled by the inner surface adsorption. In other words, the adsorption behavior for Pb^{2+} is dominated by chemical adsorption.[33]

The adsorption process was further investigated by employing the intra-particle diffusion model. Generally, in many cases the intra-particle diffusion into the interior of the adsorbent through the pores is considered to be the rate-controlling step, where the uptake amount of solutes increases almost linearly with $t^{0.5}$ rather than with the contact time t.[34] Therefore, the adsorption equation can be referred to:

$$q_t = k_{p_i} t^{0.5} + C_i \quad (4)$$

where k_{p_i} is the intra-particle diffusion rate constant at stage i (mmol g^{-1} $h^{-0.5}$). The intercept of C_i represents the thickness of boundary layer. According to the theory, q_t *versus* $t^{0.5}$ should be linear when the intra-particle diffusion occurred in the adsorption process. Otherwise, additional mechanisms may be involved. As shown in Fig. 3d, the intra-particle diffusion fitting plot for Pb^{2+} uptake into chitin/EM@Fe_3O_4 hydrogel is consist of three stages. All the linear lines for each stage did not pass through the origin, demonstrating that the intra-particle diffusion could not solely determine the overall rate of mass transfer at the initial stage of adsorption process. Both the film diffusion (chemical reaction) at the first linear region and the following pore diffusion at the second linear segments contribute to the adsorption rate. More evidence could be clarified from the Boyd's model,[35] which is given as:

$$F = 1 - \frac{6}{\pi^2}\exp(-Bt) \quad (5)$$

where F is the fractional attainment of equilibrium at different contact times t, and Bt is a function of F

$$F = \frac{q_t}{q_e} \quad (6)$$

where q_t and q_e are the amount of Pb^{2+} loaded (mmol g^{-1}) into chitin/EM@Fe_3O_4 hydrogel at time t and at equilibrium state, respectively. Then the eqn (5) could be rewritten as:

Table 1 Kinetic parameters for adsorption of Pb^{2+} into chitin/EM@Fe_3O_4 hydrogel at 20 °C in aqueous solution

Pseudo-first-order kinetics			Pseudo-second-order kinetics		
k_1 (h^{-1})	q_e (mmol g^{-1})	R_1^2	k_2 (g $mmol^{-1}$ h^{-1})	q_e (mmol g^{-1})	R_2^2
0.0034	0.0214	0.9199	0.3789	0.0467	0.9966

$$Bt = -0.4977 - \ln(1 - F) \quad (7)$$

The rate-controlling step in the adsorption process of Pb^{2+} into chitin/EM@Fe_3O_4 hydrogel will be easily distinguished from the Boyd plots. If the values of Bt change linearly along with the incubation time t and pass through the origin, the rate of mass transfer is controlled by the pore diffusion. If the plot profile is nonlinear or linear without passing through the origin, the film diffusion or chemical reaction will mainly dominate the adsorption rate. As illustrated in Fig. 3e, the fitting plot for the adsorption process of Pb^{2+} exhibit the nonlinear behavior, clearly indicating that the film diffusion or chemical reaction is the rate-limiting step in the initial period and then follows the intra-particle diffusion.

3.3 Adsorption isotherms of Pb^{2+} into chitin/EM@Fe_3O_4 hydrogel

The adsorption efficiency strongly depends on the initial concentration of heavy metal ions in solution. Usually, the adsorption capacity is enhanced along with the increase of the concentration of metal ions in the solution.[31] As shown in Fig. 4a, the amount of Pb^{2+} (q_e) adsorbed into chitin/EM@Fe_3O_4 hydrogel increased from 0.013 to 0.070 mmol g^{-1}, when the initial concentration of Pb^{2+} increased from 0.7 to 18.0 mmol L^{-1} at 293 K. This relationship between the adsorption capacity at the fixed temperature and the ions concentration at equilibrium can be easily described by the equilibrium adsorption isotherms, including the Langmuir and Freundlich equations. It is of great importance to learn more about the mutual interactions and optimize the dosage of adsorbents. The Langmuir isotherm model is established in the following form:[31]

$$\frac{1}{q_e} = \frac{1}{q_{max}} + \frac{1}{q_{max} b} \cdot \frac{1}{c_e} \quad (8)$$

where q_{max} (mmol g^{-1}) is the maximum adsorption capacity associated with the monolayer coverage on the surface, and b is the Langmuir constant (L $mmol^{-1}$), reflecting the uptake efficiency. Unlike Langmuir model, the Freundlich isotherm is supposed to be an empirical equation to study the multilayer adsorption process on heterogeneous surface:[36]

$$\ln q_e = \frac{1}{n} \ln c_e + \ln K_F \quad (9)$$

where K_F is the Freundlich constant, and the exponent $1/n$ is the heterogeneity factor, indicating the adsorption capacity and intensity, respectively.

Fig. 4b and c present the Langmuir and Freundlich profiles for Pb^{2+} adsorption in absorbents at 293 K, respectively, and the

Table 2 Langmuir and Freundlich parameters for Pb^{2+} adsorption into chitin/EM@Fe_3O_4 hydrogel at 20 °C in aqueous solution

Langmuir parameters			Freundlich parameters		
q_{max} (mmol g^{-1})	B (L $mmol^{-1}$)	R^2	$1/n$	K_F (mmol g^{-1})	R^2
0.079	0.259	0.9727	0.542	0.017	0.9301

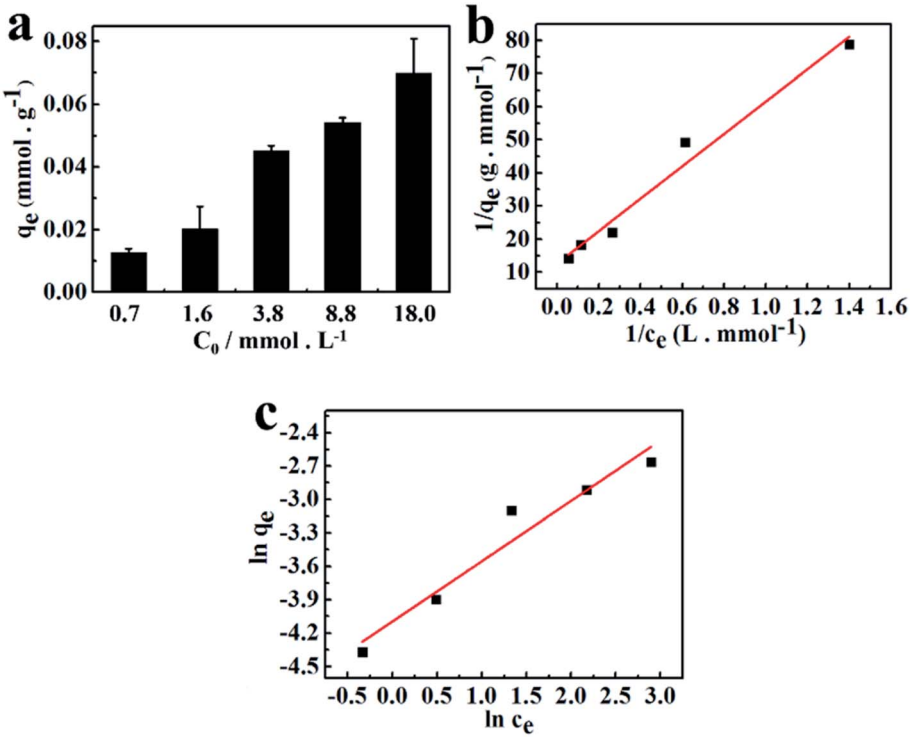

Fig. 4 (a) Adsorption isotherms for Pb^{2+} adsorption on chitin/EM@Fe_3O_4 hydrogel at 20 °C in pH = 5 aqueous solution. The related Langmuir isotherms (b) and (c) Freundlich isotherms for Pb^{2+} adsorption in chitin/EM@Fe_3O_4 hydrogel.

related parameters are summarized in Table 2. In Langmuir model, the value of q_{max} was estimated to be 0.079 mmol g^{-1}, implying that the as-fabricated chitin/EM@Fe_3O_4 nanocomposite hydrogel could display high adsorption capacity for Pb^{2+} in aqueous solution. As for the Freundlich plot fitting, the value of $1/n$ was determined to be 0.542 at 293 K, revealing that Pb^{2+} could be easily anchored into the absorbents. In Freundlich equation, the constant $(1/n)$ is closely related to the adsorption intensity of the adsorbent. When the value of $1/n$ ranges $0.5 < 1/n \leq 1$, adsorbates are easy to be anchored on the matrix.[37] Based on the fact that the regression coefficient of R^2 obtained from the Langmuir model ($R^2 = 0.9727$) is higher than that for the Freundlich model ($R^2 = 0.9301$), it can be concluded that the uptake process of Pb^{2+} into the chitin/EM@Fe_3O_4 hydrogel prefers to the Langmuir adsorption. Namely, the adsorption process in water solution is primarily dominated by monolayer adsorption.

3.4 Thermodynamic parameters of Pb^{2+} adsorption

Fig. 5a depicts the effects of incubation temperature on the uptake capacity for Pb^{2+} adsorption into chitin/EM@Fe_3O_4 hydrogel in water solution. The equilibrium adsorption capacity slightly increased from 0.043 to 0.050 mmol g^{-1}, as the temperature was elevated from 4 to 37 °C, revealing the endothermic nature of this adsorption process. With the aim to intensively explore the endothermic nature in the adsorption process, the thermodynamic parameters, such as standard free energy (ΔG°), enthalpy change (ΔH°) and entropy change (ΔS°) are determined by utilizing the following equations[38]:

$$\Delta G^\circ = -RT \ln K_d \quad (10)$$

$$K_d = \frac{1000\, q_e}{C_e} \quad (11)$$

The values of ΔH° and ΔS° can be calculated by van't Hoff equation:

$$\ln K_d = \frac{\Delta S^\circ}{R} - \frac{\Delta H^\circ}{RT} \quad (12)$$

where K_d is the standard thermodynamic equilibrium constant at the absolute temperature of T (K), R is the gas constant (8.314 J mol^{-1} K^{-1}).

As shown in Table 3, the value of ΔG° for Pb^{2+} adsorption into chitin/EM@Fe_3O_4 hydrogel was negative, indicating that the adsorption of Pb^{2+} into absorbents underwent a favorable and spontaneous process. The decreased value of ΔG° with an increase in temperature suggests that the higher temperature is beneficial to the Pb^{2+} adsorption in solution. Furthermore, according to the linear fitting profile of $\ln K_d$ *versus* $1/T$ (Fig. 5b), the values of ΔH° and ΔS° in water solution were determined to be 48.6 kJ mol^{-1} and 267.3 J mol^{-1} K^{-1}. The positive value of ΔH° demonstrates the endothermic nature of the adsorption process and the existence of an energy barrier. The large positive value of ΔS° proves the higher binding ability of Pb^{2+} to the nanocomposite matrix and the increased randomness at the solid–solution interface.[39]

3.5 Effects of pH on Pb^{2+} adsorption behavior

Plenty of function groups such as the hydroxy, amino, carboxyl, acetyl amino and hemiacetal groups exist in the chitin/EM@Fe_3O_4 nanocomposite hydrogel. The protonation/deprotonation of these groups is susceptible to the environmental pH conditions. Therefore, pH plays an important role in regulating the adsorption behavior for metal ions. To avoid the precipitation of Pb^{2+} in higher condition, the pH values of the solutions were adjusted within the range of 1.0–5.0 for investigation. As illustrated in Fig. 6, the as-prepared adsorbent performs different behaviors for Pb^{2+} adsorption during the pH ranges. The adsorption capacity increased sharply as the pH value increased from 1.0 to 5.0. The zeta potentials for the

Table 3 Thermodynamic parameters for Pb^{2+} adsorption into chitin/EM@Fe_3O_4 hydrogel at 20 °C in aqueous solution

Temperature (K)	ΔH° (kJ mol^{-1})	ΔS° (J mol^{-1} K^{-1})	ΔG° (kJ mol^{-1})
277	48.6	267.3	−5.58
293			−6.05
310			−6.74

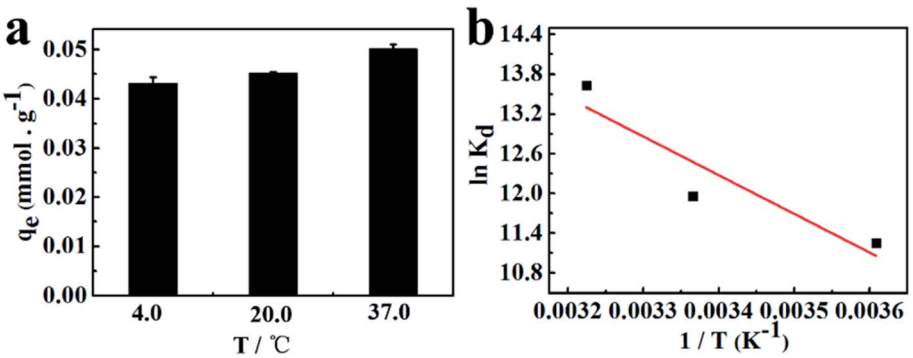

Fig. 5 (a) Effects of temperature on uptake capacity of Pb^{2+} adsorption into chitin/EM@Fe_3O_4 hydrogel at 20 °C in pH = 5 aqueous solution. (b) The corresponding Van't Hoff plots for Pb^{2+} adsorption in chitin/EM@Fe_3O_4 hydrogel.

hydrogel samples are positive (Fig. S2†), revealing that the amino groups are protonated in the whole pH range. This occurrence would result in the electrostatic repulsive force with Pb^{2+} and prevent the metal complex formation. Hence, the increase in adsorption capacity is mainly relevant to the deprotonation of the carboxyl groups and the electronegative oxygen atoms in hydroxy, acetyl amino and hemiacetal groups. In condition of low pH, the protonation of active sites such as carboxylates takes place, which is unfavorable for the Pb^{2+} binding to the biosorbents. Meanwhile, abundant hydrogen ions (H^+) will restrain the activity of electronegative oxygen, thus leading to the decrease in adsorption capacity.[40] As the pH increases, the ionization of –COOH groups from the citric stabilized Fe_3O_4 nanoparticle and EM protein occurred, and in turn the increased negative charges of $–COO^-$ groups will give rise to the stronger binding ability to heavy metal ions.[41] Moreover, the lone pair of electrons in the neutral oxygen atoms (the hemiacetal oxygen atom of the anhydro-glucose at the non-reducing end and the hydroxyl groups of an anhydro-glucose unit at the reducing end) under high pH condition is beneficial to the formation of coordination bonds between O atoms and the lead atoms.[42]

3.6 Regeneration

As an ideal adsorbent, how to recover and maintain the original adsorption capacity is vital for the practical application. In this study, Pb^{2+}-loaded nanocomposite hydrogels were regenerated by using 0.05 mol L^{-1} HCl aqueous solution. For comparison, 0.1 mol L^{-1} EDTA aqueous solution was also introduced as another static eluting agent. Since the component of Fe_3O_4 nanoparticles in chitin/EM@Fe_3O_4 nanocomposite hydrogel may be dissolved or chelated in the eluting solution, the weight loss of Fe was firstly explored. According to the original and final weight contents of Fe in hydrogel samples, the weight loss can be calculated as:

$$\mathrm{Loss_{Fe}} = \frac{m_0(\mathrm{Fe}) - m_t(\mathrm{Fe})}{m_0(\mathrm{Fe})} \quad (13)$$

where m_0(Fe) (g) is the original weight content of Fe in hydrogel sample, and m_t(Fe) (g) is the weight content of Fe after incubating the hydrogel sample in the eluting solution for the given time of t. As shown in Fig. 7, after immersing the hydrogel samples in the eluting agents of diluted HCl and EDTA aqueous solutions for 48 h, the corresponding loss amounts of Fe from the matrix were evaluated to be 10.6% and 5.7%, respectively. The values of weight loss for the hydrogel samples in HCl aqueous solution are relatively higher than those in EDTA aqueous solution, implying that the nanocomposite biosorbents displayed higher stability in EDTA solution during the regenerated process. Although the phenomena of weight loss would occur in both cases, the values are acceptable and can still be utilized as the candidate eluting agents. Alternatively, in order to maximally reduce the weight loss of Fe during the regeneration, the elution time can be limited to be 0.5–1 h in each cycle, which has been demonstrated to be sufficient to remove the adsorbed heavy metal ions from the matrix. Similar processing methods have been readily applicated in the regeneration of various adsorbents, such as Fe_3O_4/sawdust carbon,[43] Fe_3O_4-modified sugarcane bagasse[44] or CMC/alginate/graphene oxide@Fe_3O_4.[45]

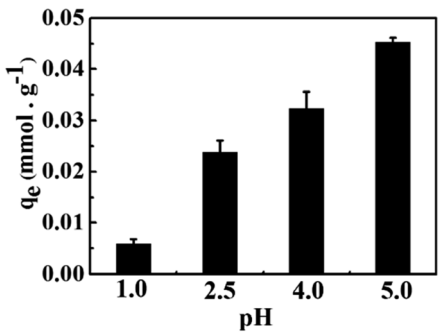

Fig. 6 Effects of pH on the uptake capacity of Pb^{2+} adsorption in chitin/EM@Fe_3O_4 hydrogel at 20 °C in aqueous solution.

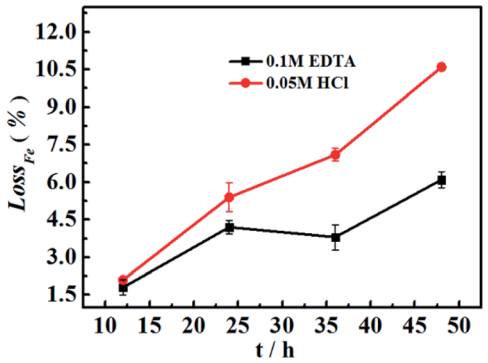

Fig. 7 The weight loss of Fe as a function of immersing time for chitin/EM@Fe_3O_4 hydrogel samples in different eluting media at 20 °C.

Further, the regeneration behaviors were investigated. As listed in Table 4, the desorption ratios of Pb^{2+} from the matrix by using EDTA aqueous solution were slightly higher than diluted HCl solution in each cycle, confirming the better elution ability. Irrespective of the experimental deviation, these results reveal that most of the Pb^{2+} adsorbed in chitin/EM@Fe_3O_4 hydrogel could be removed in both cases, testifying the potential re-usability of the adsorbents. When the regenerated materials were placed in Pb^{2+} aqueous solution upon the same

Table 4 Repeated adsorption capacity and desorption efficiency of Pb^{2+} into chitin/EM@Fe_3O_4 hydrogel in the desorption–regeneration cycle

Cycle number	Adsorption capacity (mmol g^{-1})	Desorption efficiency (%)
HCl-1	0.0453	88.96
HCl-2	0.0403	92.01
HCl-3	0.0387	81.27
EDTA-1	0.0467	94.43
EDTA-2	0.0436	94.21
EDTA-3	0.0407	92.17

incubation condition, they displayed a slight decrease tendency in the loading efficiency after each cycle. The existence of the small and reasonable decrease in adsorption capacity may be due to the static elution method, resulting in the incomplete desorption of ions from the matrix. In spite of this, the developed chitin/EM@Fe_3O_4 hydrogel could still be a good candidate for future application.

4. Conclusion

A novel kind of chitin/EM@Fe_3O_4 nanocomposite hydrogel derived from the biowastes of egg shell membrane and chitin was successfully prepared from the NaOH/urea aqueous system. The obtained hydrogel adsorbent could display the enhanced adsorption efficiency for Pb^{2+} in aqueous solution with the addition of egg shell membrane and citric stabilized Fe_3O_4 nanoparticles in the matrix. The good correlation coefficient (0.9966) demonstrates that the adsorption process in water solution obeys the pseudo-second-order kinetic model, implying that the Pb^{2+} uptake into the hydrogel is mainly controlled by the inner surface adsorption. Moreover, the adsorption behaviors strongly depend on the initial concentration of the Pb^{2+}, pH value and the incubation temperature. The adsorption process of Pb^{2+} into this absorbent can be suitably described by the Langmuir isotherm, and the thermodynamic analysis indicates that the adsorption behavior was spontaneous and endothermic. In addition, the nanocomposite bio-sorbents could still display high uptake capacity after three cycles. This work will pave a way for the utilization of novel biomass-based absorbents for rapid and high-capacity removal of heavy metal ions.

Conflicts of interest

There are no conflicts to declare.

Acknowledgements

Dr Qy Liu gratefully acknowledges the financial support from Natural Science Foundation of China (51603195). Jie Ren thanks Postgraduate Education Innovation Project of Shanxi Province, China (2020SY400).

References

1 Y.-M. Liu, X.-J. Ju, Y. Xin, W.-C. Zheng, W. Wang, J. Wei, R. Xie, Z. Liu and L.-Y. Chu, *ACS Appl. Mater. Interfaces*, 2014, **6**, 9530–9542.
2 H. N. Kim, W. X. Ren, J. S. Kim and J. Yoon, *Chem. Soc. Rev.*, 2012, **41**, 3210–3244.
3 X.-J. Ju, S.-B. Zhang, M.-Y. Zhou, R. Xie, L. Yang and L.-Y. Chu, *J. Hazard Mater.*, 2009, **167**, 114–118.
4 I. Hajdu, M. Bodnár, Z. Csikós, S. Wei, L. Daróczi, B. Kovács, Z. Győri, J. Tamás and J. Borbély, *J. Membr. Sci.*, 2012, **409**, 44–53.
5 S. Liang, X. Guo, N. Feng and Q. Tian, *J. Hazard. Mater.*, 2009, **170**, 425–429.
6 X. He, D.-P. Yang, X. Zhang, M. Liu, Z. Kang, C. Lin, N. Jia and R. Luque, *Chem. Eng. J.*, 2019, **369**, 621–633.
7 X. Li, J. Xing, C. Zhang, B. Han, Y. Zhang, T. Wen, R. Leng, Z. Jiang, Y. Ai and X. Wang, *ACS Sustainable Chem. Eng.*, 2018, **6**, 10606–10615.
8 S. Abbaszadeh, S. R. W. Alwi, C. Webb, N. Ghasemi and I. I. Muhamad, *J. Clean. Prod.*, 2016, **118**, 210–222.
9 N. Nematidil, M. Sadeghi, S. Nezami and H. Sadeghi, *Carbohydr. Polym.*, 2019, **222**, 114971.
10 J. Jiang, Y. Long, X. Hu, J. Hu, M. Zhu and S. Zhou, *J. Solid State Chem.*, 2020, **289**, 121491.
11 R.-S. Wang, Y. Li, X.-X. Shuai, R.-H. Liang, J. Chen and C.-M. Liu, *Polymers*, 2021, **13**, 2453.
12 Q. Sun, B. Aguila, J. Perman, L. D. Earl, C. W. Abney, Y. Cheng, H. Wei, N. Nguyen, L. Wojtas and S. Ma, *J. Am. Chem. Soc.*, 2017, **139**, 2786–2793.
13 M. Basu, A. K. Guha and L. Ray, *J. Clean. Prod.*, 2017, **151**, 603–615.
14 N. Feng, X. Guo, S. Liang, Y. Zhu and J. Liu, *J. Hazard Mater.*, 2011, **185**, 49–54.
15 D. Sud, G. Mahajan and M. P. Kaur, *Bioresour. Technol.*, 2008, **99**, 6017–6027.
16 S. Park, K. S. Choi, D. Lee, D. Kim, K. T. Lim, K.-H. Lee, H. Seonwoo and J. Kim, *Biosyst. Eng.*, 2016, **151**, 446–463.
17 B. Liu and Y. Huang, *J. Mater. Chem.*, 2011, **21**, 17413–17418.
18 A. Mittal, M. Teotia, R. Soni and J. Mittal, *J. Mol. Liq.*, 2016, **223**, 376–387.
19 M. N. R. Kumar, *React. Funct. Polym.*, 2000, **46**, 1–27.
20 Y. Zhong, J. Cai and L.-N. Zhang, *Chin. J. Polym. Sci.*, 2020, 1–14.
21 L. Qiao, L. Zhao and K. Du, *Chem. Eng. J.*, 2020, **393**, 124818.
22 D. Liu, Y. Zhu, Z. Li, D. Tian, L. Chen and P. Chen, *Carbohydr. Polym.*, 2013, **98**, 483–489.
23 Y. Duan, A. Freyburger, W. Kunz and C. Zollfrank, *ACS Sustainable Chem. Eng.*, 2018, **6**, 6965–6973.
24 G. I. Tovar Jimenez, A. Valverde, C. Mendes-Felipe, S. Wuttke, A. Fidalgo-Marijuan, E. S. Larrea, L. Lezama, F. Zheng, J. Reguera and S. Lanceros-Méndez, *ChemSusChem*, 2021, **14**, 2892–2901.
25 B. Duan, Y. Huang, A. Lu and L. Zhang, *Prog. Polym. Sci.*, 2018, **82**, 1–33.
26 R. Singh and R. Bhateria, *ACS Omega*, 2020, **5**, 28305–28318.
27 J. Duan, X. He and L. Zhang, *Chem. Commun.*, 2015, **51**, 338–341.
28 M. He, Z. Wang, Y. Cao, Y. Zhao, B. Duan, Y. Chen, M. Xu and L. Zhang, *Biomacromolecules*, 2014, **15**, 3358–3365.
29 T. Hou, H. Zhang, D. He, Q. Liu, Z. Zhang, L. Xiao, W. Li and M. Barnes, *RSC Adv.*, 2018, **8**, 36858–36868.
30 J. Liu, Z. Sun, Y. Deng, Y. Zou, C. Li, X. Guo, L. Xiong, Y. Gao, F. Li and D. Zhao, *Angew. Chem., Int. Ed.*, 2009, **48**, 5875–5879.
31 H. Tang, W. Zhou and L. Zhang, *J. Hazard Mater.*, 2012, **209**, 218–225.
32 H. Tu, M. Huang, Y. Yi, Z. Li, Y. Zhan, J. Chen, Y. Wu, X. Shi, H. Deng and Y. Du, *Appl. Surf. Sci.*, 2017, **426**, 545–553.
33 A. S. Özcan and A. Özcan, *J. Colloid Interface Sci.*, 2004, **276**, 39–46.

34 B. Hameed, I. Tan and A. Ahmad, *J. Colloid Interface Sci.*, 2008, **144**, 235–244.
35 A. Özcan, E. M. Öncü and A. S. Özcan, *J. Hazard Mater.*, 2006, **129**, 244–252.
36 G. Bayramoglu, A. Denizli, S. Bektas and M. Y. Arica, *Microchem. J.*, 2002, **72**, 63–76.
37 B. Samiey and M. R. Dargahi, *Cent. Eur. J. Chem.*, 2010, **8**, 906–912.
38 D. Ding, Y. Zhao, S. Yang, W. Shi, Z. Zhang, Z. Lei and Y. Yang, *Water Res.*, 2013, **47**, 2563–2571.
39 X.-F. Sun, S.-G. Wang, X.-W. Liu, W.-X. Gong, N. Bao, B.-Y. Gao and H.-Y. Zhang, *Bioresour. Technol.*, 2008, **99**, 3475–3483.
40 K. Zhang, Z. Li, N. Deng, J. Ju, Y. Li, B. Cheng, W. Kang and J. Yan, *Cellulose*, 2019, **26**, 945–958.
41 Z. P. Li, X. R. Duan, C. H. Liu and B. A. Du, *Anal. Biochem.*, 2006, **351**, 18–25.
42 F. Zhao, E. Repo, Y. Song, D. Yin, S. B. Hammouda, L. Chen, S. Kalliola, J. Tang, K. C. Tam and M. Sillanpää, *Green Chem.*, 2017, **19**, 4816–4828.
43 N. Kataria and V. Garg, *Chemosphere*, 2018, **208**, 818–828.
44 G. Liu, L. Liao, Z. Dai, Q. Qi, J. Wu, L. Q. Ma, C. Tang and J. Xu, *Chem. Eng. J.*, 2020, **395**, 125108.
45 Z. Wu, W. Deng, W. Zhou and J. Luo, *Carbohydr. Polym.*, 2019, **216**, 119–128.